Supplemental Information for "Crumpled Kirigami"

Wathsala M.A. Jayawardana[a], Yangchao Liao[b], Zhaofan Li[b], Wenjie Xia[b,c] and Andrew B. Croll[a,c]

Overview of sheet model being cut and molecular dynamics simulations

Based on our previously developed CG graphene model,[1] we performed coarse-grained molecular dynamics (CG-MD) simulations to explore the crumpling and uniaxial compression behaviors of graphene sheets with cuts. Informed from the underlying atomic graphene model, as shown in Figure S1a, the employed CG model of graphene is derived based on a 4-to-1 mapping scheme to preserve the hexagonal lattice geometry, where each CG bead with a mass of $48\ g/mol$ represents four carbon atoms. As listed in Table S1, the CG force field of the CG model includes bonded interactions, *i.e.*, bonds $V_b(d)$, angles $V_a(\theta)$, dihedrals $V_d(\phi)$, and pairwise non-bonded interactions $V_{nb}(r)$. Specifically, the bond, angle, and dihedral interactions are used to describe the elastic modulus and fracture strength, shear modulus, and bending rigidity of the graphene sheet respectively; the adhesion energy of the sheet is captured by the pair-wise non-boned interaction. Further details on the development of the CG model can be found in the earlier study.[1]

[a] Department of Physics, North Dakota State University, Fargo, USA.
[b] Department of Civil, Construction and Environmental Engineering, North Dakota State University, Fargo, ND, USA.
[c] Materials and Nanotechnology, North Dakota State University, Fargo, USA.

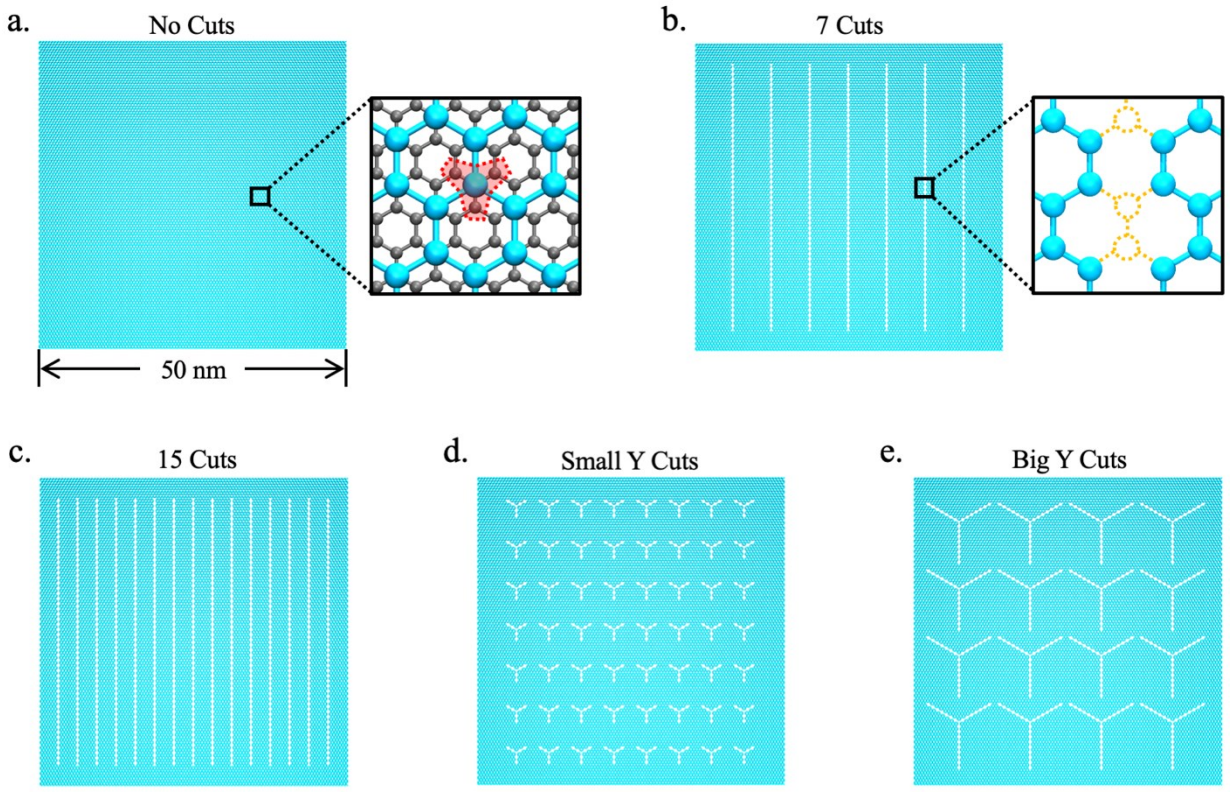

Figure S1. Representation of CG models of graphene sheets with different cutting patterns (kirigami patterns), i.e., a.) no cuts, b.) 7 cuts, c.) 15 cuts, d.) small Y cuts, and e.) big Y cuts, respectively. The zoom-in in a.) shows the 4-to-1 mapping scheme of the CG graphene model, where the four connected carbon atoms (black atoms) are grouped into a CG bead (cyan bead) as highlighted in the red region. The zoom-in in b.) shows the cut pattern created by deleting the specific CG beads (orange dashed open circles).

Table S1. Functional forms and interaction parameters of the CG graphene model.

Interaction	Function form	Parameters
Bond	$V_b(d) = D_0[1 - e^{-\alpha(d-d_0)}]^2$ for $d < d_{cut}$	$D_0 = 196.38\ kcal/mol$ $\alpha = 1.55\ Å^{-1}$ $d_0 = 2.8\ Å$ $d_{cut} = 3.25\ Å$
Angle	$V_a(\theta) = k_\theta(\theta - \theta_0)^2$	$k_\theta = 409.4\ kcal/mol$ $\theta_0 = 120°$
Dihedral	$V_d(\phi) = k_\phi[1 - cos(2\phi)]$	$k_\phi = 4.15\ kcal/mol$
Non-bonded	$V_{nb}(r) = 4\varepsilon\left[\left(\frac{\sigma}{r}\right)^{12} - \left(\frac{\sigma}{r}\right)^{6}\right]$ for $r < r_{cut}$	$\varepsilon = 0.82\ kcal/mol$ $\sigma = 3.46\ Å$ $r_{cut} = 12\ Å$

In this study, we investigated the internal structure and compressive strength of crumpled graphene sheets without cutting (no cuts) and with 7 cuts, 15 cuts, small Y cuts and big Y cuts patterns (Figure S1). All the MD simulations are carried out using an open-source software

package Large-scale Atomic/Molecular Massively Parallel Simulator (LAMMPS),[2] and the visualization of the MD simulation is achieved by Visual Molecular Dynamics (VMD).[3] Specifically, the energy minimization, equilibrium simulation, and crumpling simulation of the sheet are carried out sequentially before uniaxial compression and unloading simulations. First, the square graphene sheet with an edge length of $50\ nm$ is placed horizontally (xy-plane) in the center of the simulation box, which has dimensions of $500\ nm \times 500\ nm \times 500\ nm$; the periodic boundary conditions are applied to the system in all directions, with time step and simulated temperature of $6\ fs$ and $300\ K$, respectively. The iterative conjugate gradient algorithm is utilized for the energy minimization,[4] and $2\ ns$ of NVT ensemble is simulated for the equilibrium of the system, which results in the final convergence of the total potential energy of the system to a nearly constant value.

Then, as shown in Figure S2, the crumpling process is achieved by crumpling the sheet with a confining sphere containing the model. That is, a repulsive force $F_c(r_i)$ from the boundary of confining sphere is applied to the sheet within a certain cutoff distance when the sheet is inside the confining sphere. The confining force $F_c(r_i)$ can be written as:

$$F_c(r_i) = \{-K_c(r_i - R_c)^2, for\ r_i \geq R_c\ 0, for\ r_i < R_c \quad \text{(S1)}$$

where R_c, r_i, K_c are the radius of the confining sphere, radial distance from the ith bead to the center of the confining sphere, spring force constant ($K_c = 2.31 \times 10^5\ kcal/mol/nm^3$), respectively. The crumpling process of the sheet is achieved by decreasing the radius of the confining sphere R_c at a certain speed (*i.e.*, $50\ m/s$). More details on the sheet crumpling simulations can be found in earlier studies.[5][6][7]

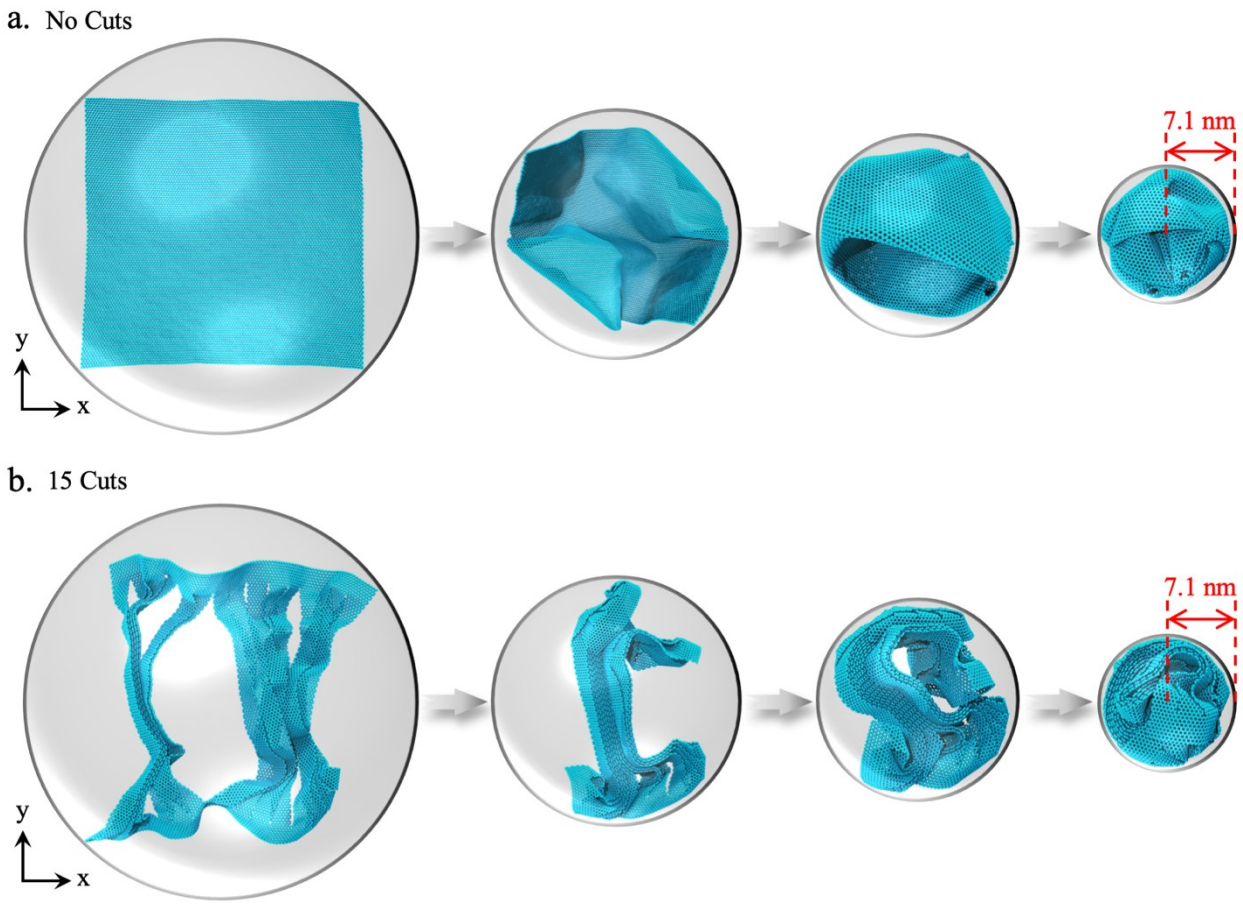

Figure S2. Schematic of the MD simulation of the crumpling process for CG graphene sheet with a.) no cuts and b.) 15 cuts. Here, a confining sphere containing the sheet model is used to compress the sheet. As the radius of the confining sphere continuously decreases, the sheet gradually gets crumpled to the final sphere-like structure with a radius of 7.1 *nm.*

It can be observed from Figure S2 that the pristine graphene sheet (no cuts) basically maintains a flat configuration in the initial equilibrium state, and it shows significant edge bending and self-folding behaviors during the crumpling process, which can also be learned from our previous studies.[5][7] Interestingly, for the graphene sheet with 15 cuts, it develops a stacked lamellar structure due to adhesion in the initial equilibrium state, and the stacking behavior intensifies and finally compresses into a crumpled sphere upon crumpling. It is evident that at the molecular level, the cutting controls the final crumpled structure of the graphene sheet by affecting its initial configuration and crumpling behavior.

Upon obtaining the final crumpled spherical structure, we further conduct uniaxial compression and unloading simulations. To simulate the compression and unloading tests in the

experiment, we replace the confining sphere with a confining cylinder of equal radius, whose height is equal to the diameter of the confining sphere. As shown in Figure S3, while maintaining the crumpled state (cyan) in the confining cylinder, two parallel rigid plates (gray) are added at the two ends of the z-axis at a distance $3.46\,\text{Å}$ from the crumpled model, both of which are $20\,nm \times 20\,nm$ in size and the same material properties as the crumpled model. Afterward, the compression and unloading simulation of the crumpled model is achieved by defining a specific moving speed for the two plates with opposite or opposing directions, respectively. We specify the minimum separation between the two plates to be roughly $5\,nm$, which is to disregard the non-bonded interactions between the plates. When applying equation $F = Et^2(2R_0/H)^\alpha$, we choose parameter σ of the non-boned interaction as the thickness t of the model, where $\sigma = 3.46\,\text{Å}$ is a length scale parameter related to the equilibrium distance of two nonbonded beads. In our study, thirteen different compression speeds ranging from $40\,m/s$ to $100\,m/s$ are employed and ten independent simulations are performed for each compression speed, to obtain the average value of the target properties of the crumpled model with different cutting patterns.

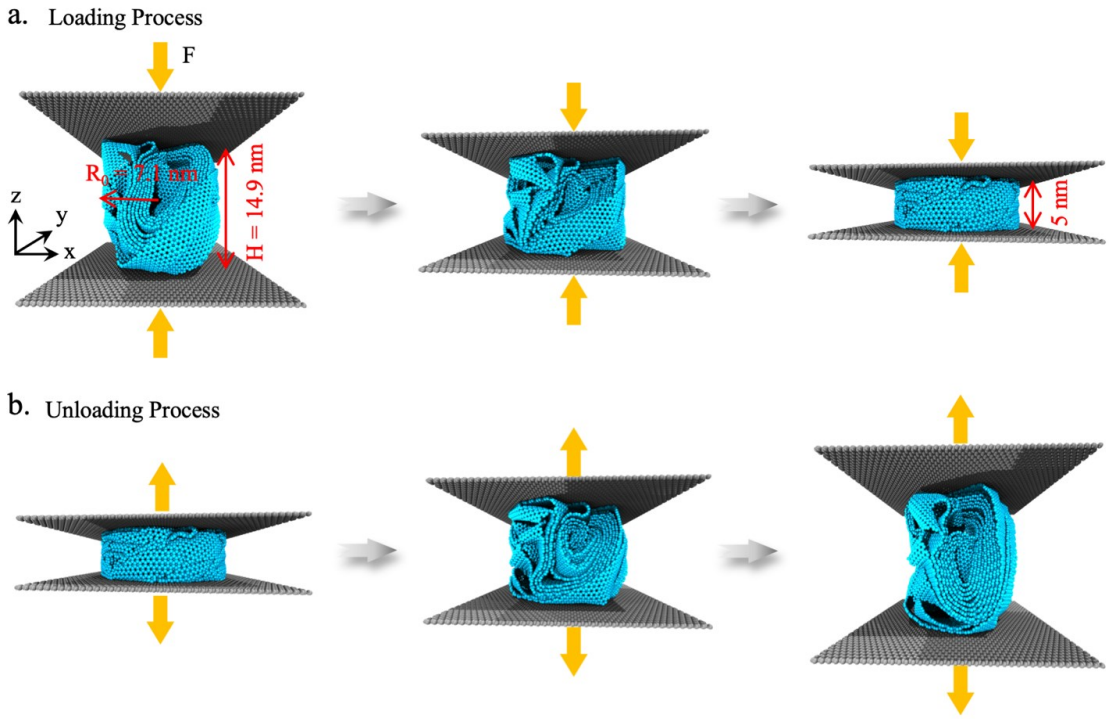

Figure S3. Schematics of the MD simulations for a.) uniaxial compression and b.) unloading simulations. Here, the crumpled sheet with a radius of R_0 ($R_0 = 7.1\ nm$) is disposed between two rigid and parallel plates; the separation between the two plates is H. The compression and unloading simulations of the crumpled model is achieved by defining a specific moving speed for the two plates with opposite or opposing directions, respectively.

Discussion of line statistics

In our manuscript we discuss mainly the angular distribution of highly curved features fit by straight line segments. We do so because our analysis of both the experimental and simulated lines contain unavoidable error, and the angular distribution is the least affected by these errors. Error occurs because all high curvature structures may not form straight lines (though we fit with line segments), may not abruptly start or stop (they may taper beyond where our line segments fit), and may fluctuate in curvature from one end to the other (i.e. is it one long line or two short line segments oriented in the same direction?). Both programs used in analysis would thus have to make choices deal with these issues that will always be, in some view, imperfect. This said, data generated by these two separate analysis programs (one for simulations, one for experiments) is still meaningful, though in a more qualitative sense. Therefore, we present some additional detail of the distributions here for the interested reader.

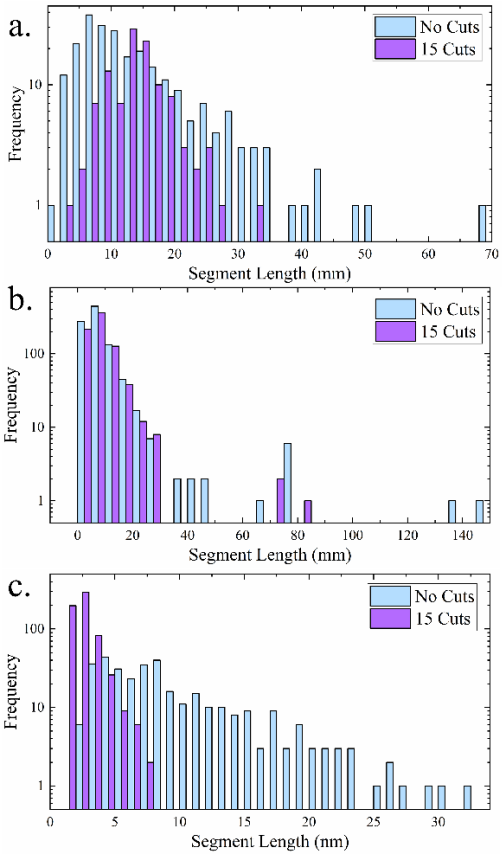

Figure S4. Histograms of high curvature segment lengths. a. A low density crumpled paper sheet, both uncut and cut 15 times. The cut sample shows a reduced 'tail' of longer length structures. b. A high density paper crumple. Again, a reduction in long segments is evident. c. Segments from a typical MD simulations. Simulations also show a large reduction in long segments when cuts are present.

Figure S4 shows typical distributions of lengths of high curvature structures for low density, high density and simulated crumples. For all data we see a similar loss of long structures in cut sheets, directly vindicating the main goal of our study. Interestingly, the distributions are fairly similar between cut and uncut films at smaller line lengths. The higher density data of the simulations, however, shows a peak at lower line lengths for cut sheets than uncut sheets. We believe that the difference is likely related to the plasticity of the paper sheets. In short, they are much less free to re-arrange as additional stress is added to the system.

Additionally, both the number of segments and the total length of high curvature segments is larger in uncut sheets when compared to cut sheets at similar densities. Given that there is some evidence that the total length of high curvature features correlates with the effective stiffness of crumpled matter, this observation can explain the small differences in effective modulus observed in our study [8]. In summary, cuts affect the structure of the high-curvature network within a crumple by changing the angular distribution and removing long range structure, but does not significantly change the overall mechanics of the crumpled sheet.

Discussion of total line length

Gottesman et. al [8] have noted that the total line length (of creases measured in uncrumpled sheets similar to what is presented in this manuscript) correlates well with the compressive behaviour of a crumple. Unsurprisingly we also find that the total length of lines is proportional to the peak density of the crumple (note: density for us is more reasonable than a scaled gap as in [8] because we do not fix radius as they do). While Gottesman et al. only examined pristine sheets, we find very little difference with the cut sheets, save that the lengths at comparable densities are slightly smaller. As the simulations define “lines” differently than the experiment, the trends are slightly different as one would expect. Figure S5 shows the basic result.

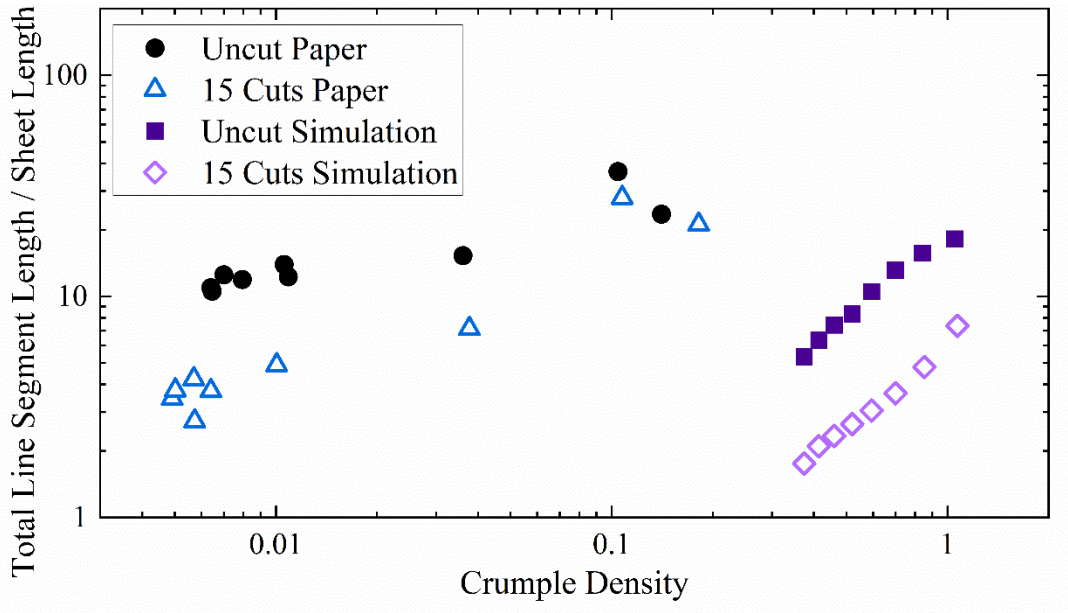

Figure S5. Total line length as a function of crumple density. Both paper and simulated data show an upward trend with density. Simulations and paper crumples differ because the way a line is measured differs between the two.

Discussion of d-cone populations

It is difficult to define, from the uncrumpled sheet, where exactly d-cones may have been at the point of peak compression. However, it is reasonable to assume this number would be proportional to the number of line-ends observed in the analysis of the uncrumpled sheet. One observes that many lines will begin or end on a cut or sheet edge, which would likely mean that one d-cone has escaped the sheet and exists only virtually. Given this hypothesis, it is then possible to examine changes in the population of d-cones by simply examining the marked sheets (in experiment or theory).

As a preliminary step in such an analysis, Figure S6 shows the fraction of virtual to total d-cones in cut and uncut sheets. Uncut sheets at various crumpled densities tend to have less than 5% of lines interacting with a sheet edge. On the other hand, cut sheets typically have somewhere between 40% to 90% of lines interacting with an edge, trending to higher numbers at lower density. Clearly the "current" location of d-cones is not significant to the crumple's resistance to compression as, once again, very little difference is noted in terms of macroscopic compression of the crumple. This is not inconsistent with the conceptual model discussed in the manuscript, because the folds still represent the path a d-cone has taken through the sheet.

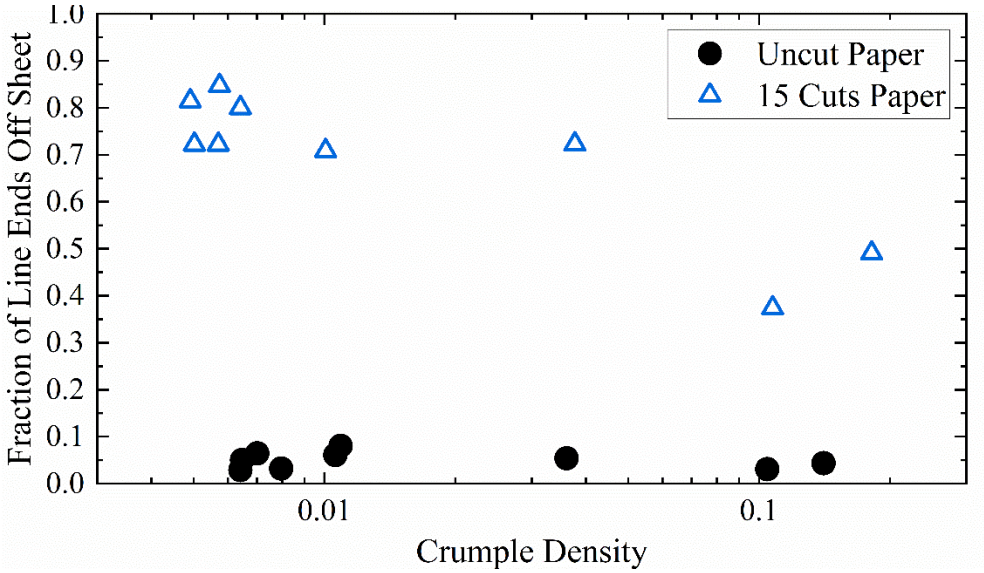

Figure S6. Fraction of line ends occurring off the sheet as a function of crumple density.

Discussion of statistical tests

In the main manuscript we claim to see very little difference between cut and uncut crumpled sheets based on subjective observation of quantitative data extracted from force-displacement curves. However, while clear from observing the presented raw data, for example, the distribution of power-law fit exponents, some readers might be unsatisfied without a quantitative measure. Therefore, we present here a quantitative verification of our conjecture by considering p-test results comparing the null hypothesis (cut sheets are not statistically different from uncut sheets) with the data. Specifically, we consider distributions of power-law fit exponents (α) between cut and uncut sheets. For paper, we find (using a Wilcoxon rank sum test implemented in MatLab) that p = 0.80 when comparing the power-law exponent of cut and uncut paper crumples. This indicates that there is no significant difference between the two populations as the p value is considerably above any typical cut-off (say p=0.05). For polycarbonate we find p = 0.38 and in the simulations we find $p = 1.27\times10^{-34}$. Thus, only the simulations have the statistical power to clearly differentiate the two populations, likely due to the incredible control of sample-to-sample variation possible in a simulation.

References

[1] L. Ruiz, W. Xia, Z. Meng, and S. Keten, "A coarse-grained model for the mechanical behavior of multi-layer graphene," *Carbon N. Y.*, vol. 82, no. C, pp. 103–115, 2015, doi: 10.1016/j.carbon.2014.10.040.

[2] S. Plimpton, "Fast parallel algorithms for short-range molecular dynamics," *J. Comput. Phys.*, vol. 117, no. 1, pp. 1–19, 1995, doi: 10.1006/jcph.1995.1039.

[3] W. Humphrey, A. Dalke, and K. Schulten, "VMD: Visual molecular dynamics," *J. Mol. Graph.*, vol. 14, no. 1, pp. 33–38, 1996, doi: 10.1016/0263-7855(96)00018-5.

[4] M. C. Payne, M. P. Teter, D. C. Allan, T. A. Arias, and J. D. Joannopoulos, "Iterative minimization techniques for ab initio total-energy calculations: Molecular dynamics and conjugate gradients," *Rev. Mod. Phys.*, vol. 64, no. 4, pp. 1045–1097, 1992, doi: 10.1103/RevModPhys.64.1045.

[5] Y. Liao, Z. Li, Fatima, and W. Xia, "Size-dependent structural behaviors of crumpled graphene sheets," *Carbon N. Y.*, vol. 174, pp. 148–157, 2021, doi: 10.1016/j.carbon.2020.12.006.

[6] Y. Liao, Z. Li, S. Ghazanfari, Fatima, A. B. Croll, and W. Xia, "Understanding the Role of Self-Adhesion in Crumpling Behaviors of Sheet Macromolecules," *Langmuir*, vol. 37, no. 28, pp. 8627–8637, 2021, doi: 10.1021/acs.langmuir.1c01545.

[7] Y. Liao, Z. Li, W. Nie, and W. Xia, "Effect of reconstructed vacancy defects on the crumpling behavior of graphene sheets," *Forces Mech.*, vol. 6, p. 100057, 2022, doi: 10.1016/j.finmec.2021.100057.

[8] O. Gottesman, J. Andrejevic, C.H. Rycroft, et al. "A state variable for crumpled thin sheets." *Commun. Phys*. vol. 1, pp. 70, 2018,